Intermetallics 121 (2020) 106794

Contents lists available at ScienceDirect

Intermetallics

journal homepage: http://www.elsevier.com/locate/intermet

Indirectly probing the structural change in ion-irradiated Zr-Based metallic glasses from small scale mechanical tests

Tingkun Liu [a], Wei Guo [b], Miguel L. Crespillo [a], Ke Jin [c], Yanwen Zhang [a,d,**], Hongbin Bei [e,***], Yanfei Gao [a,*]

[a] Department of Materials Science and Engineering, University of Tennessee, Knoxville, TN, 37996, USA
[b] Center for Nanophase Materials Sciences, Oak Ridge National Laboratory, Oak Ridge, TN, 37831, USA
[c] School of Materials Science and Engineering, Beijing Institute of Technology, Beijing, 100081, PR China
[d] Materials Science and Technology Division, Oak Ridge National Laboratory, Oak Ridge, TN, 37831, USA
[e] School of Materials Science and Engineering, Zhejiang University, Hangzhou, 310058, PR China

ARTICLE INFO

Keywords:
Metallic glasses
Ion irradiation
Nanoindentation pop-in
Micropillar compression
Irradiation induced defects
Heterogeneities

ABSTRACT

Ion irradiation was applied to tailor the structural heterogeneities in Zr-based metallic glasses at room temperature. Experimental methods of X-ray diffraction, nanoindentation, and micropillar compression were conducted to examine the irradiation effects on their structural and mechanical property changes. It is found that the irradiated materials retained amorphous structure after room-temperature Ni ion irradiation. The reduction of elastic modulus and hardness measured by nanoindentation indicated the irradiation-induced mechanical degradation. A unified statistic model was employed to quantitatively predict the density and strength of irradiation defects, although their specific structural and physical nature is not explicitly included in this model. The transition of non-intersecting shear bands to multiple intersecting shear bands was observed on compression tests of irradiated micropillars with the increase of irradiation dose. The analysis of the displacement excursion of micropillar compression tests indicated a different deformation mode from the unirradiated state. These results from nanoindentation pop-in and micro-pillar compression tests suggested that irradiation eventually leads to a new state with different types and characteristics of structural heterogeneities from violent displacement cascades and non-equilibrium energy deposition/dissipation processes, which also proves ion irradiation as an effective method to tune the structure and mechanical properties of metallic glasses.

1. Introduction

Due to the amorphous structure that lacks the long-range order and geometric defects such as grain boundaries and dislocations, metallic glasses (MGs) have shown unique mechanical properties such as high strength, high fracture toughness, good corrosion resistance and formability [1–3]. On the other hand, metallic glasses as structural materials have the notorious problem of poor ductility at temperatures below the glass transition temperature, T_g. A tendency towards catastrophic failure at room temperature is characterized by localized plastic shear bands, which has not been clearly linked to a specific well-defined microstructural feature, in contrast to the dislocations in crystalline metals. Nevertheless, deformation theories must have a connection to the atomic structural description; candidate measures include the free volume, shear transformation zone (STZ), and effective temperature [4–6]. Generally, it is well accepted that the shear band trends to initiate at local structural heterogeneity described as high free volume zones, liquid-like zones [7] or soft spots [8], which are usually defined as defects in MGs. While the ductility of MGs can be enhanced by introducing second phases and geometric constraints to block the propagation of shear bands [9], it is these structural inhomogeneities or defects that should be investigated and tuned in regards of the intrinsic ductility of MGs. Usually, both thermal processing and mechanical loading can introduce such structural inhomogeneities, resulting in various levels of ductility improvement [10,11]. It has been reported that non-affine thermal strain is utilized to improve room-temperature compressive

* Corresponding author.
** Corresponding author.Department of Materials Science and Engineering, University of Tennessee, Knoxville, TN, 37996, USA.
*** Corresponding author.
E-mail addresses: yanwen@utk.edu (Y. Zhang), hbei2018@zju.edu.cn (H. Bei), ygao7@utk.edu (Y. Gao).

https://doi.org/10.1016/j.intermet.2020.106794
Received 18 January 2020; Received in revised form 19 March 2020; Accepted 26 March 2020

plasticity which is attributed to thermal cycling induced rejuvenation with the evolution of heterogeneities during thermal cycling [12]. A mechanical relaxation-to-rejuvenation transition of Zr-base bulk metallic glass (BMG) was observed through elastic compression at ambient temperature [13], which states that stress-driven structural change of defects (e.g., loosely packed regions and densely packed regions) could be achieved. All the above observations reveal that the dynamic structure of MGs can be tailored by thermally and mechanical induced rejuvenation, resulting from the change of structural disordering, be it described by the free volume, the fictive temperature, or others.

Irradiation could be another approach to tailoring the amorphous structure in an alternative way to thermal processing and mechanical loading, since the bombardment of MGs with energetic particles such as electrons, neutrons, and ions induces structural heterogeneities [14–16]. Energetic charged particles (ion beams) have been used to investigate defect kinetics and dislocation dynamics under non-equilibrium or far-from equilibrium conditions. Ion beams create very localized (i.e., a few nanometers) supersonic shockwaves with extremely high pressures (e.g., 10–50 GPa) and temperatures (e.g., several thousands of degrees Kelvin). Specifically, ion-solid interactions along ion paths generate high-energy recoils. The evolution of high-energy displacement cascades processes leads to atomic displacements that eventually result in either localized defect production and structural damage, or atomic re-arrangement and new phase formation [17–19]. Recently, in the experimental investigation of the mechanical response of molded MG nanowires subjected to ion irradiation, a transition from originally brittle-like to ductile-like tensile behavior was found as a direct result of the structural change [20]. In this study, the observed increase of ductility and reduction of yield strength were understood by changes in the fictive temperature, and the resultant mechanical softening proved that the material was changed to a different structure state by ion irradiation. These irradiation-induced defects assist the formation of shear bands, similar to the thermally and mechanically induced structural heterogeneities. In another study, X-ray diffraction (XRD) and transmission electron microscopy (TEM) have demonstrated that the dynamic structure of MGs could be changed under low-dosage irradiation by increasing the free volume and homogenizing its distribution, which is equivalent to decreasing in the yield strength by increasing the deformation temperature [21]. On the contrary, irradiation induced hardening has also been observed in many MGs, among which nanocrystallization is believed to be responsible for the hardness increase [22,23]. Overall speaking, few direct observations of irradiation-induced defects were reported experimentally, despite extensive characterizations from molecular dynamics (MD) simulations. Recent MD research suggested that the plastic deformation mode of the MG nanopillars transits from localized shear banding to homogeneous shear flow due to irradiation-induced structural disordering [24]. A similar numerical study stated that ion-beam bombardment successively modifies the compositional and structural order toward a universal state, which leads to an increase in free volume and reduction of yield stress in irradiated MGs [25]. All these studies indicate that, by carefully controlling particle energy, temperature, and irradiation fluence, energetic ions can be applied as a unique tool to reduce local rearrangement and to tune the structures and properties of MGs.

As mentioned above, the macroscopic properties are related to the local structural changes due to irradiation caused by charged particles through collision and ionizing interactions. The characterization and quantification of such structural variations have been a long-term challenge, especially for low-dose early-stage ion irradiation damage, for which difficulties mainly arise from the small defect size, nonuniform damage profile, and shallow penetration depth. While the subtle changes in defect formation and evolution are hardly detectable by transmission electron diffraction constrained in the tiny local regions unless nanocrystalline phases form [20,21], their mechanical properties can be significantly affected. Statistical analysis is essential to bridge the structure and properties in such circumstances. Additionally, high-energy X-ray diffraction (HEXRD) using intense synchrotron sources has been used to detect microscopic structural modifications in atomic scales, but it is still elusive to directly quantify or correlate to the mechanical behavior [26]. Consequently, the quantitative characterization of early-stage irradiation defects is still not sufficiently investigated, especially using direct experimental methods, which brings a vast field for the exploration of the structure-property relationship.

In this work, a mechanically-based structural probing technique with high throughput capability is proposed to uncover the above scientific issues. As a nanoscale structural probing method, nanoindentation pop-in tests have been utilized to characterize structural heterogeneities quantitatively in MGs [27,28]. Pop-ins, or sudden displacement-bursts on the load-displacement curve in a nanoindentation test, are typically attributed to heterogenous dislocation nucleation sources triggered in the very small stressed volume in crystalline metals [29,30], and they correspond to structural heterogeneities associated with shear bands formation in MGs [31,32]. It is suggested that the irradiation particles change the amorphous structure inhomogeneously, so that performing statistical nanoindentation pop-in tests enables a thorough evaluation of the atomistic structural features in irradiated MG samples.

In this study, a Zr-base MG is subjected to Ni ion irradiation to different dosages to study the structural and mechanical changes by the experimental methods of XRD, nanoindentation, and micropillar compression. For nanoindentation, a unified statistic model is proposed to predict the density and strength of irradiation induced defects in MGs. For micropillar compression, direct observation of the shear band configurations and in situ monitoring of the stress-strain responses can reveal the related statistical nature of the shear banding behavior. Irradiation induced mechanical softening is observed and the transition of the amorphous state is controlled by irradiation induced defects. As a result, a different amorphous state is generated by ion irradiation which is distinguished from the relaxed state. These observations suggest that ion irradiation be an effective method for tailoring the structure and properties of MGs by introducing structural heterogeneities.

2. Experimental methods

Metallic glasses with a nominal composition of $Zr_{52.5}Cu_{17.9}Ni_{14.6}Al_{10}Ti_5$ (BAM-11) were fabricated by arc-melting a mixture of the pure base metal element in an argon atmosphere. The alloy was re-melted and formed rod-like material with a diameter of 7 mm by subsequent drop cast in a Zr-gettered helium atmosphere. The cast sample was annealed at 200 °C for 24 h for further processing. Six samples were cut by electrical discharge machining (EDM) with a thickness of 1 mm. They were then ground and finally polished by colloidal silica suspensions.

The ion irradiation experiments were conducted at the Ion Beam Materials Laboratory (IBML) located at the University of Tennessee [33]. The annealed MG samples were irradiated at room temperature with 10 MeV Ni^{3+} ions at flux 1.04×10^{12} $cm^{-2}s^{-1}$ in an area of 6×6 mm^2. The displacement ion profiles of Ni irradiation were simulated using the Stopping and Range of Ions in Matter (SRIM-2013) [34] as shown in Fig. 1. Displacements per atom (dpa) is used to measure the amount of radiation damage. SRIM simulations in the full-cascade mode [35] were used under the condition of the threshold displacement energy as 40eV and the sample density as 6.7 g/cm^3 [36]. The conversion factor from ion fluence (10^{14} cm^{-2}) to peak damage in dpa, based on the full-cascade versus quick SRIM, is 0.21 at a depth of ~3210 nm. The corresponding peak concentration of implanted Ni is 0.0018% at 3550 nm. In this study, the highest Ni fluence is 1.11×10^{16} cm^{-2} and the peak injected Ni concentration is ~0.19% (Fig. 1), which has negligible influence on the composition or chemical effects. Based on the calculation result from SRIM, the irradiation fluences vary from 1.11×10^{13} to 1.11×10^{16} ions cm^{-2} to achieve the peak doses of 0.023, 0.12, 0.46, 2.3, and 23 dpa at the depth of around 3.2 μm beneath the surface. The

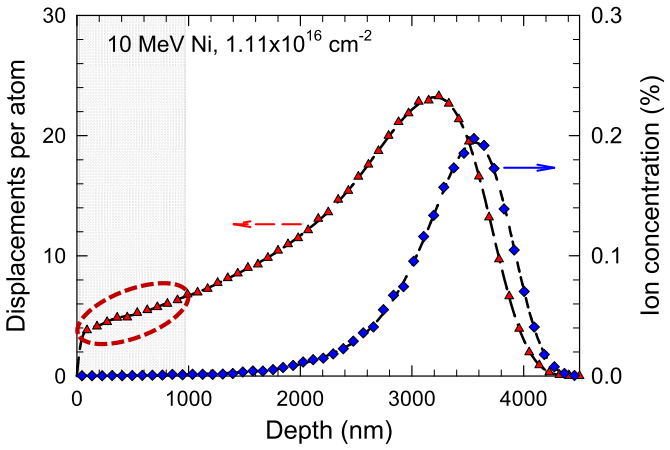

Fig. 1. Damage (triangles) and ion (diamonds) profile calculated by SRIM with full-cascade option after 10 MeV Ni ion irradiation at the highest influence of 1.1×10^{16} cm^{-2} under the assumed condition of the threshold displacement energy as 40 eV for all elements and the sample density as 6.7 g/cm^3. The dashed lines are curve fits to guide the eye. The red circle indicates the average does of the depth region (shaded area) for nanoindentation pop-in tests where the dpa is about 21.5% of the peak dose value.

applied fluences and resultant doses are summarized in Table 1. The average dose beneath surface less than 1 μm is about 21.5% of the peak dose.

Instrumented nanoindentation tests were performed at room temperature on annealed and irradiated samples using Nanoindenter® XP system equipped with a spherical indenter of radius R = 1.78 μm. All the tests were carried out in the continuous stiffness mode with a constant strain rate of 0.05 s^{-1} and holding for 10 s at peak load. The maximum load on the sample is 4 mN and the maximum depth is less than 1 μm. A total number of 120 indents were conducted on each sample, and these indents were placed far enough to avoid interference. The first pop-in load was recorded for the subsequent calculation of the maximum shear stress. The nanoindentation modulus and hardness were estimated using a simple predictive model for spherical indentation [37].

The structure of annealed and irradiated samples was investigated by XRD using a PANalytical's X-ray diffractometer with Cu-Kα radiation. The XRD is used to identify the amorphous state of MGs after annealing and irradiations.

Micropillars with an initial diameter of ~2 μm with an aspect ratio >2 were fabricated using a dual beam focused ion beam (FIB) system (FEI Nova 200) operated at a constant accelerating voltage of 30 kV. Using the top-down circular milling approach, the materials between two concentric circles can be retained. The selected beam current was gradually decreased from 6.5 nA to 86 pA when decreasing the size of the inner circle. A detailed description of the top-down milling method can be found in previous works [38,39]. Every pillar is located in a crater with about 40 μm diameter, leaving enough space for 20 μm-wide flat punch tip to avoid interference with the surrounding bulk material. The mechanical properties of the FIB-milled micropillars were measured in compression tests using a Nanoindenter® XP equipped with a flat punch diamond tip. The morphology of micropillars were examined using a tabletop scanning electron microscope (SEM) operated in the back-scattered electron (BSE) mode at an acceleration voltage of 15 kV. High-resolution SEM was conducted to observe the morphology of shear bands after compression using a field emission gun (FEG) SEM JEOL 6500 at an acceleration voltage of 20 kV.

3. Results

The XRD patterns of specimens before and after irradiation show two broaden peaks in Fig. 2, revealing fully amorphous without visible Bragg's peaks within the XRD resolution. Even the highest dose of 23 dpa does not lead to crystallization. The first diffuse peaks are fitted by pseudo-Voigt function and the full width at half maximum (FWHM) is used to characterize the structural evolution as plotted against the dosage in Fig. 3. The inset curve is the illustration of the fitting of the first diffuse peak of the annealed sample, where the red line is the fitted result, the black line is the experimental result and the arrow line indicates the FWHM. The value of FWHM rapidly increases with increasing doses from 0 to 2.3 dpa and slightly increases to 23 dpa. The evolution of FWHM suggests that the amorphous state becomes more disordered after irradiation and it changes quickly at a low dose level and then increases slowly at high doses. It can be deduced that the disorder will be saturated at a higher dose which will probably produce a disorder-to-order change.

Since the maximum depth of nanoindentation is less than 1 μm, the effective irradiation near the surface is about 1/5 of the peak dose. Thus, the nanoindentation results is discussed as a function of doses as 0, 0.0046, 0.023, 0.092, 0.46, and 4.6 dpa. The representative load-displacement curves of nanoindentation at different irradiation doses are displayed in Fig. 4. The pop-in event is regarded as the sudden

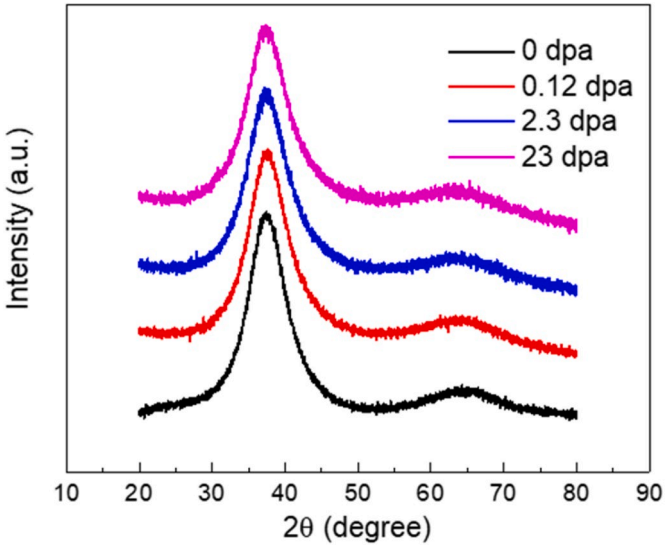

Fig. 2. XRD patterns of annealed and irradiated samples under different dosages show the first and second diffuse peaks without sharp Brag peaks within the XRD resolution, verifying the fully amorphous features of the samples and no crystallization after irradiation.

Table 1
Fluences and doses as calculated by the damage profile of Ni ion irradiation in Fig. 1.

# Sample	Fluence (cm^{-2})	Peak dose (dpa) at 3.2 μm	Average dose up to 1 μm (dpa)	Peak concentration (%) at 3.55 μm
1(annealed)	0	0	0	0
2	1.11×10^{13}	0.023	0.005	0.00019
3	5.56×10^{13}	0.12	0.025	0.00097
4	2.22×10^{14}	0.46	0.1	0.0039
5	1.11×10^{15}	2.3	0.5	0.019
6	1.11×10^{16}	23	5	0.19

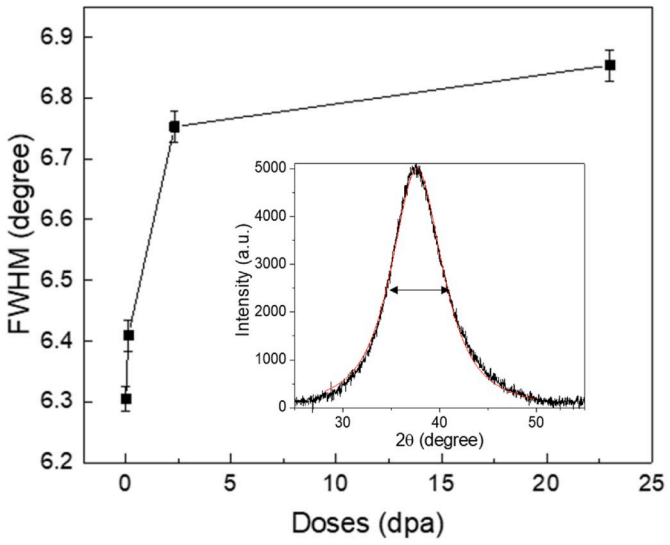

Fig. 3. Full width at half maximum (FWHM) of annealed and irradiated samples as a function of irradiation doses. The inset is the illustration of peak fitting by pseudo-Voigt function and FWHM of the first diffuse peak.

displacement excursion highlighted by the black circle on the load-displacement curves, whereas the first pop-in represents the initiation of plastic deformation and formation of the first shear band. The pop-in events were observed in each nanoindentation test of the samples with doses of 0, 0.0046, and 0.023 dpa. However, pop-in events were not observed in approximately half of 120 nanoindentation tests on the sample under an irradiation dose of 0.092 dpa. Interesting, pop-ins vanished in all the nanoindentation tests for samples under doses of 0.46 and 4.6 dpa. With the increase of irradiation doses, the pop-ins are more difficult to detect mainly because of the irradiation-induced high-density defects to assist the formation of the shear band, so the displacement burst is smaller than the instrument resolution. As a result, the pop-ins disappeared in the nanoindentation tests of highly irradiated samples. Even without direct microstructural evidences, one can presume that the deformation in such highly irradiated regions presents a different regime and is seemingly homogeneous.

The load at the first pop-in is denoted as P_{pop-in}, which is used to calculate the maximum shear stress τ_{max} under the spherical nanoindentation by [40].

$$\tau_{max} = 0.445\left(\frac{16P_{pop-in}E_r^2}{9\pi^3R^2}\right)^{1/3} \quad (1)$$

where E_r is the reduced modulus, and $R = 1.78$ μm is the radius of the spherical indenter. The reduced modulus E_r is determined by $E_r = [(1-\nu_s^2)/E_s + (1-\nu_i^2)/E_i]^{-1}$, where E_s, ν_s, E_i and ν_i are Young's moduli and Poisson ratios of samples and diamond indenter, respectively. The maximum shear stress τ_{max} of the first pop-in is statistically analyzed as shown in Fig. 5. The box displays the average, maximum, minimum and standard deviation of the distribution of τ_{max}. It can be clearly seen that the annealed sample possesses the highest averaged τ_{max} value of about 3.26 GPa. The averaged τ_{max} reduces to about 2.91 GPa with the increase of dose up to 0.092 dpa. The annealed sample shows the largest τ_{max} distribution, which indicates that the plastic deformation of the unirradiated sample is the most inhomogeneous. The standard deviation of τ_{max} in 0 dpa sample reveals the inhomogeneous deformation. After irradiation, the stresses required for the onset of plastic deformation decreased, and the deformation becomes more homogeneous.

The hardness and the reduced modulus were estimated by a simple predictive model for spherical indentation [37]. The schematic illustration in Fig. 6 shows the relationship between the depth of loaded and unloaded indentations. The radius of the circle of contact is calculated from $a = \sqrt{2Rh_p - h_p^2}$, where h_p is the depth of penetration below the circle of contact. Meyer's hardness is defined as the mean pressure over the circle of contact. Hence, the hardness can be calculated from the load P and the radius of the contact circle a by $H = P/\pi a^2$. The indentation depth, δ, can be obtained from the depth below the original surface during both loading and unloading, which are termed as h_t and h_r, representatively. Assuming the elastic displacement is evenly divided above and below the circle of contact, the relationship of h_t, h_r, δ and h_p is given as $h_t = h_r + \delta = h_p + \delta/2$. Fig. 6 displays the hardness and modulus as a function of irradiation doses. The hardness of the 0 dpa sample is 5.9 GPa and the modulus is 116.9 GPa. The irradiation up to 0.023 dpa does not affect the hardness and modulus. The transition is found at the irradiation dose of 0.092 dpa. Further irradiation significantly reduces the hardness and modulus. At the peak dose level, the hardness decreases by 22% and the modulus decrease by 15%. Therefore, the high dose irradiation could induce mechanical degradation in these samples, and the softening is significant above the dose of 0.092 dpa.

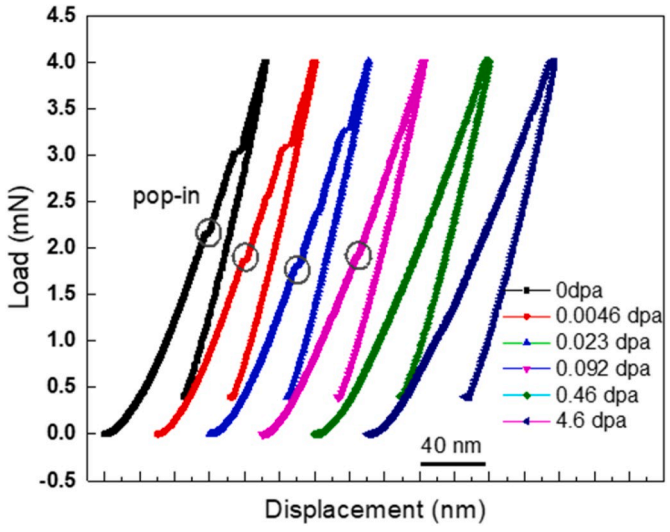

Fig. 4. Representative load-displacement curves of nanoindentation pop-in tests at different irradiation dosages. The black circles indicate the first pop-ins, which gradually disappear as the dosage increases to 0.46 dpa and 4.6 dpa due to high density defects and limitation of instrument resolution.

To further understand the mechanism for the irradiation induced softening, the cumulative probability τ_{max} is analyzed in Fig. 7 at different doses of 0, 0.0046, 0.023 and 0.092 dpa using dot plotting. The cumulative probability curves shift leftward to low stress value. The slopes of cumulative probability curves of 0.0046 dpa and 0.023 dpa samples are similar, but different from those of 0 dpa and 0.092 dpa sample. The curve profile of the unirradiated sample presents a larger tail at low stress level compared with 0.0046 dpa and 0.023 dpa samples. The difference of the cumulative probability curves at varying doses derives from irradiation induced structural heterogeneities, which is investigated by a proposed model in the following.

A unified statistic model is employed to quantitatively correlate the irradiation structural heterogeneities to the cumulative probability, resulting from a synergy between the thermally activated homogeneous nucleation process and the pre-defect-assisted heterogeneous process. Specifically, the nucleation process is pointed out to be a well-known deformation mechanism. Governed by the homogeneous process, the shear bands nucleate until the applied stress τ exceeds the theoretical shear stress τ_{th}. The equation $\dot{n} = \dot{n}_0 \exp[(\tau v^* - \varepsilon)/kT]$ determines the nucleation rate, where $\dot{n}_0$ is a pre-factor, v^* is the activation volume, T is the absolute temperature, ε is the intrinsic nucleation energy barrier, and k is Boltzmann constant. Homogeneous survivability q_{homo} that

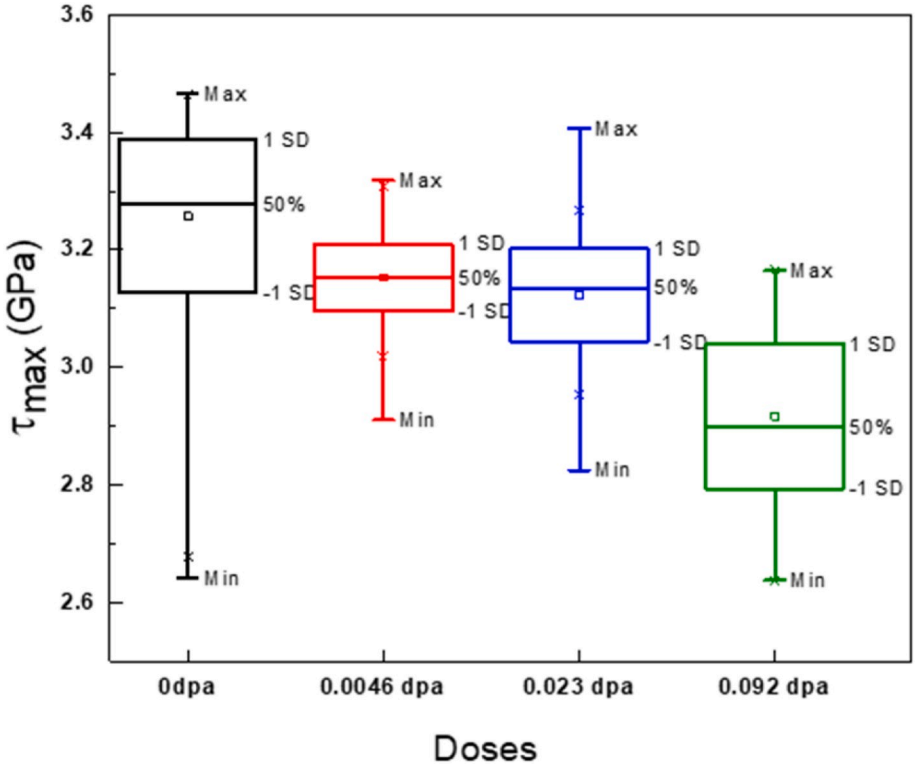

Fig. 5. Box plots of the maximum shear stresses (τ_{max}) of first pop-ins at different doses with mean value, median, minimum, maximum and standard deviation (SD) showing the tendency of τ_{max} and deformation inhomogeneity as a function of doses.

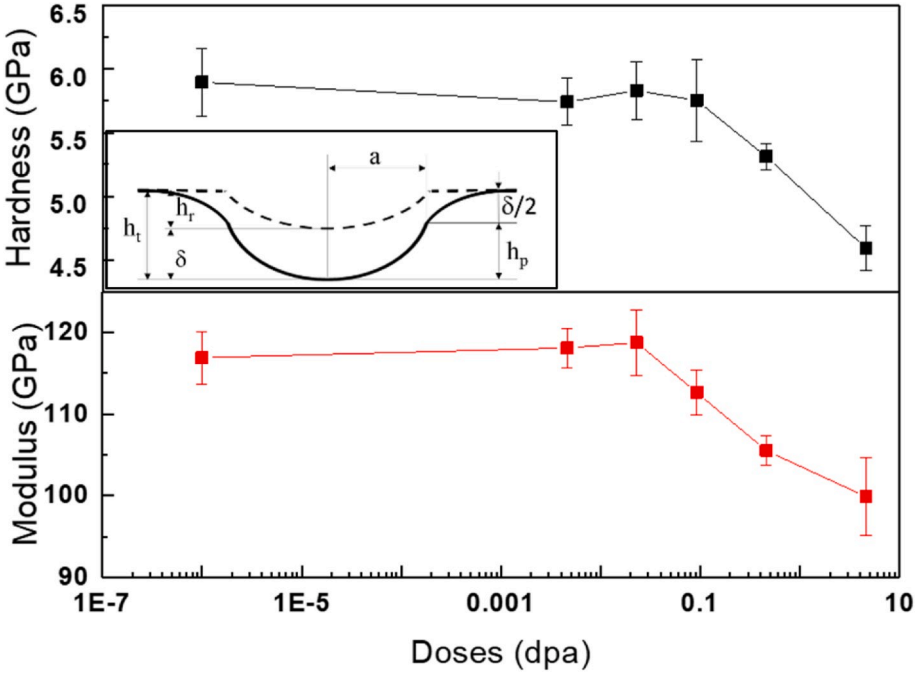

Fig. 6. Hardness and modulus as a function of doses estimated by nanoindentation tests using a simple model of spherical indentation. The inset is illustration of the relationship between the depth of loaded and unloaded indentations.

represents the probability of no homogeneous defect nucleation is given by

$$q_{homo} = \exp\left(A_0 \int_{-\infty}^{\tau_{eff}^{pop-in}} \exp\left(\frac{\tau_{eff} v^*}{kT}\right) \frac{1}{\tau_{eff}} d\tau_{eff}\right) \quad (2)$$

where A_0 and v^* are fitting parameters. Thus, the cumulative probability for homogeneous shear band nucleation process is simply written as $f_{homo} = 1 - q_{homo}$. The heterogeneous shear band formation process is governed by pre-existing defects, i.e., the structural heterogeneities in MGs. It is assumed that the first pop-in will occur if the applied stress is

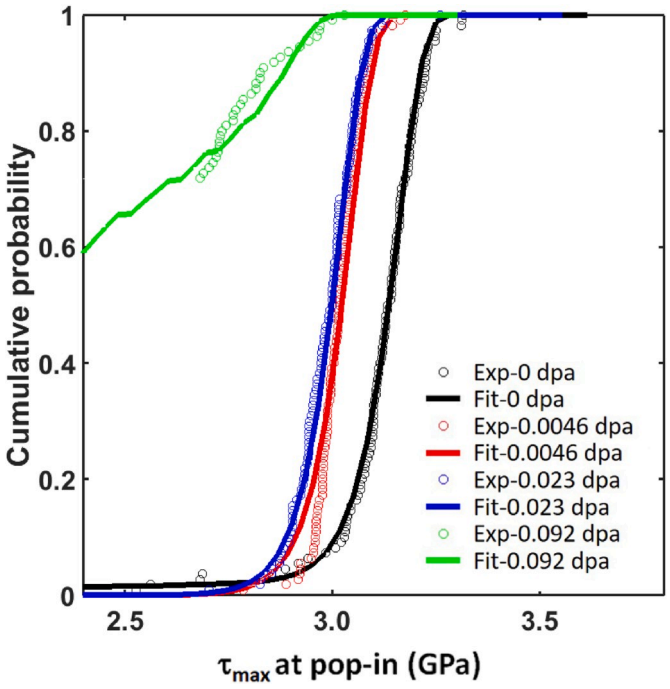

Fig. 7. Plots of cumulative probability and fitting curves of τ_{max} of first pop-in at different irradiation doses, where the dots represent experimental data and the solid lines are fitting results by the unified statistical model.

larger than the defect strength τ_{def} in a given volume V_d, within which a pre-existing defect is discovered. For simplicity, the value of defect strength τ_{def} is given by the bulk flow stress as the initial trial value for curve fitting. The probability of no defects found in V_d distributes by Poisson function

$$q_{hetero} = \exp\left(-\rho_{defect} V_d\right) \tag{3}$$

The given volume V_d is determined by a dimensionless analysis $V_d/a^3 = \hat{V}_d(\tau_{def}/\tau_{max})$ with a being the contact radius [29]. The values of ρ_{defect} and τ_{def} are fitted and updated in the prediction. Hence, the cumulative probability for a heterogeneous shear band formation process is determined by $f_{hetero} = 1 - q_{hetero} = 1 - \exp(-\rho_{defect} V_d)$. Considering that the homogeneous process and heterogeneous process as two independent events, the total survivability is $q_{total} = q_{hetero} \times q_{homo}$. Consequently, the unified cumulative pop-in probability is given by $f_{total} = 1 - q_{total}$ and further simplified as

$$f_{total} = 1 - \exp\left(-A_0 I\left(v^* \tau_{eff}^{pop-in} \Big/ kT\right) - \rho_{defect} V_d\right) \tag{4}$$

The exponential integral I is defined by $I(t) = \int_{-\infty}^{x} t^{-1} e^t dt$.

The fitting results by the above model are presented in Fig. 7 as solid lines, which reasonably predict the experimental investigation, except for the result of the sample irradiated to 0.092 dpa at the bottom. The corresponding fitting parameters are given in Table 2, where it is clearly seen that the irradiation increases the defect density. Specifically, the defect density is 2.2×10^{16} m^{-3} for the unirradiated sample. In this case, the pop-in event of this sample is governed by the thermally activated homogeneous nucleation and the pre-defect-assisted heterogeneous process at the same time. As a result, the cumulative probability curve shows an enhanced tail at a lower stress level. However, the pop-in events are dominated by the defects after irradiation. The irradiation induced defects have a higher strength than the intrinsic defects retained from the prior thermal processing. As more irradiation is applied, the defect density continues to increase, but the strength of irradiation induced defects reduces. Due to the extensive defects induced by irradiation, the defect spacing is decreased as illustrated in Table 2.

Table 2
Fitting parameters of the unified model corresponding to the plots in Fig. 7. The defect spacing is calculated by $1/\sqrt[3]{\rho_{defect}}$.

Samples	V* (nm^3)	A_0 ($\times 10^{-22}$)	τ_{def} (GPa)	ρ_{def} (m^{-3})	Defect spacing (um)
0 dpa	0.0685	5.96	1.14	2.2×10^{16}	3.57
0.0046 dpa	0.0726	3.32	2.58	5×10^{17}	1.26
0.023 dpa	0.0707	4.40	2.51	1×10^{18}	1.00
0.092 dpa	0.0758	4.38	1.56	5×10^{18}	0.585

Consequently, the pop-in evens are completely controlled by the defect-assisted heterogeneous processes since each indent encounters the irradiated induced defects in the stressed volume below the indenter.

Since most pop-ins of the 0.092 dpa sample and those irradiated to higher doses are not detectable due to the machine limitation, micropillars were fabricated to investigate the deformation mechanism thoroughly by compression tests. Representative micropillars before compression at each irradiation level are presented in Fig. 8. The micropillars were carefully milled by FIB with the diameter in the range of 1.87–2.32 μm. The aspect ratio (height/diameter) is constrained within 2.62–3.67. The dimensional details of all the micropillars are given in Table 3.

The compressive engineering stress-strain curves are shown in Fig. 9 at the irradiation level of 0, 0.12, 0.46, 2.3, and 23 dpa. The SEM images of each compressively deformed micropillars are overlaid in these plots. The engineering stress and strain values were determined from the measured force on the micropillar F, and the displacement Δh of the micropillar by $\sigma = 4F/\pi d^2$ and $\varepsilon = \Delta h/h$, where d is the diameter of micropillar in the position of 1/3 to the top and h is the height of the micropillar. As shown in Fig. 9, before the onset of displacement, the curves all exhibit predominantly elastic behavior on loading up to the transition of elastic to plastic deformation. Since the machine stiffness is not calibrated, the absolute value of elastic modulus is not discussed here. Shear band formation is the expected mode of deformation at high stresses, which gives rise to a displacement excursion accordingly to the stress-strain curve. The largest displacement excursion is observed on the stress-strain curve of the unirradiated sample in Fig. 9(a), indicating the formation of a major shear band immediately leads to a catastrophic failure. Except for this sample, multiple small-displacement excursions are observed. However, micropillar compression tests on the sample irradiated to 0.46 dpa exhibits smooth stress-strain curves with hardly detectable displacement excursions, indicating a structural transition occurred at a certain irradiation level. After inspecting the geometry of shear bands in Fig. 10, it is found that multiple parallel shear bands formed in the same direction in the samples irradiated below 0.46 dpa, whereas the shear band intersection is observed in the samples irradiated at higher dpa.

4. Discussion

It is well known in crystalline materials that irradiation by a single atom displacement could induce Frenkel defects, or interstitial vacancy pairs based on the assumption that every atom received energy greater than a certain threshold displaces from its lattice site and remains a vacancy permanently [41]. Such irradiation defects in MGs, which are often described as a pair of free volume defect and anti-free volume defect or interstitial-like and vacancy-like defects, result in density fluctuation [14,42]. Crystallization is also observed in some MGs after irradiation, which usually results in mechanical hardening [32,43,44]. In the current study, even the irradiation dose is applied up to 23 dpa, there is no crystalline phase observed on the XRD pattern in Fig. 2. At the same time, the observed mechanical softening such as the decrease in hardness and modulus evidently excludes the likelihood of nanocrystalline formation even without high-resolution TEM. Hence, it is

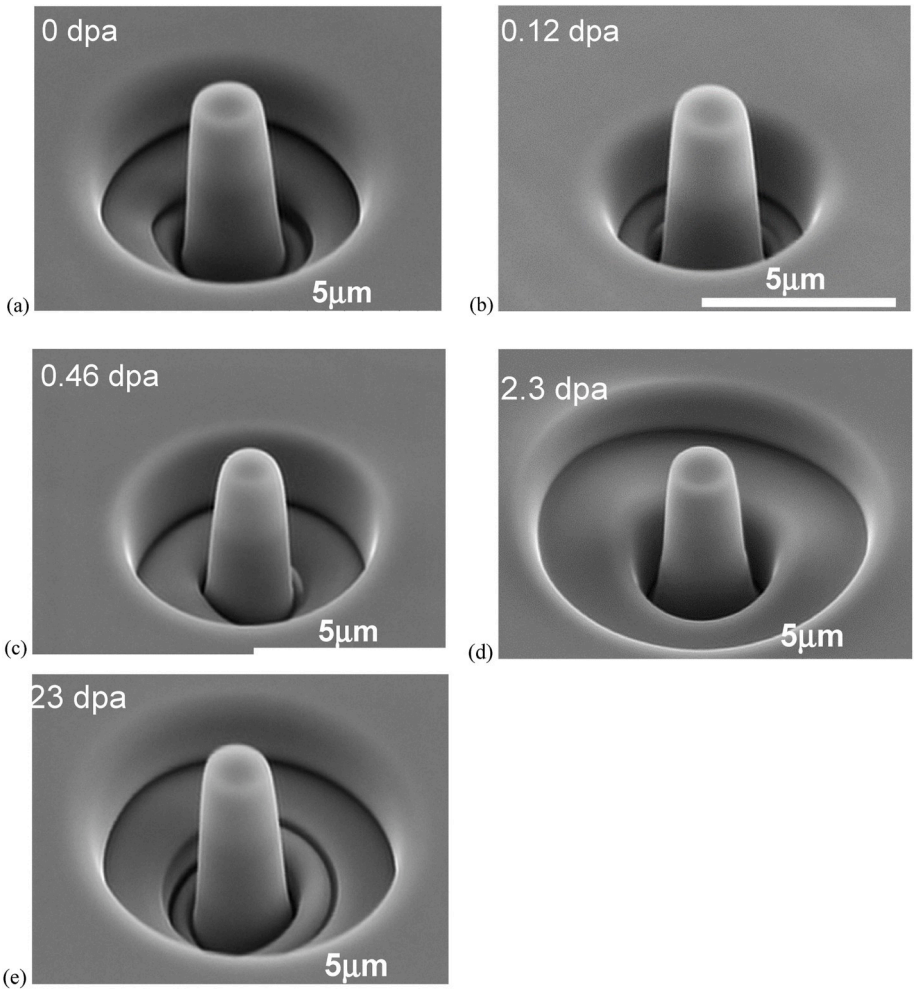

Fig. 8. Representative micropillars at different doses (a) 0 dpa to (b) 0.12 dpa, (c) 0.46 dpa, (d) 2.3 dpa and (e) 23 dpa before compression showing high-quality cylinders milled by FIB. One of three micropillars of each irradiation doses are illustrated here.

Table 3
Dimension of the FIB-milled micropillars at different irradiation doses. The micropillars were carefully milled with the diameter in the range of 1.87–2.32 μm and the aspect ratio (height/diameter) constrained within 2.62–3.67.

Peak Dose	Pillar #.	Diameter(mm)	Height(mm)	Aspect ratio
0 dpa	p1	2.29	6.70	2.93
	p2	2.31	6.38	2.76
	p3	2.07	7.20	3.48
0.12 dpa	p1	2.15	6.64	3.09
	p2	2.27	6.94	3.23
	p3	1.98	6.69	3.38
0.46 dpa	p1	1.87	5.73	3.07
	p2	2.02	5.97	2.96
	p3	2.17	5.17	2.38
2.3 dpa	p1	2.35	5.84	2.49
	p2	2.42	6.72	2.78
	p3	1.99	5.37	2.69
23 dpa	p1	2.17	5.69	2.62
	p2	2.18	6.16	2.83
	p3	2.00	7.33	3.67

proposed that a new state with different types and characteristics of structural heterogeneities is induced by ion irradiation based upon the mechanical changes of nanoindentation pop-in tests and micropillar compressions.

Mechanical softening can also be caused by thermal processing [10], plastic deformation [45], profuse shear banding [46], and residual stresses [47]. The hardness reduction reported in the above research is less than 10%. Even the combination of shear band and residual stresses does not reduce the hardness of more than 15% [47]. Compared with inhomogeneous softening caused by the above approaches in the same materials and some other MGs, the irradiation in the current work results in a higher decrease in hardness as much as 22%.

To further understand the underlying mechanism of irradiation induced mechanical softening, Fig. 11 schematically illustrates the irradiation induced defects and the structural changes after irradiation, which is referred to as "irradiation-induced rejuvenation". The intrinsic defects are directly retained from thermal history such as annealing. As a result of nanoindentation pop-in tests, the shear band formation at first pop-in is controlled jointly by thermally activated nucleation and pre-existing-defect-assisted nucleation [27,28]. The micropillars exhibit brittle-like deformation as the formation of the main shear band causes immediate failure. After ion bombardment, newly formed defects distinguish from the intrinsic defects because the defect strength is increased according to the fitting results from the proposed unified model of cumulative probability as previously shown in Fig. 7. Because of the high defect density and corresponding small defect spacing, the heterogeneous nucleation of first pop-in is easily triggered by irradiation defects. In agreement with Fig. 7, the shear band formation is dominated by irradiation induced defects in the sample irradiated to a low dose level. These high-density defects promote the shear band formation and the intersection of multiple shear bands performs ductile-like compressive deformation. More defects generate as the irradiation dose

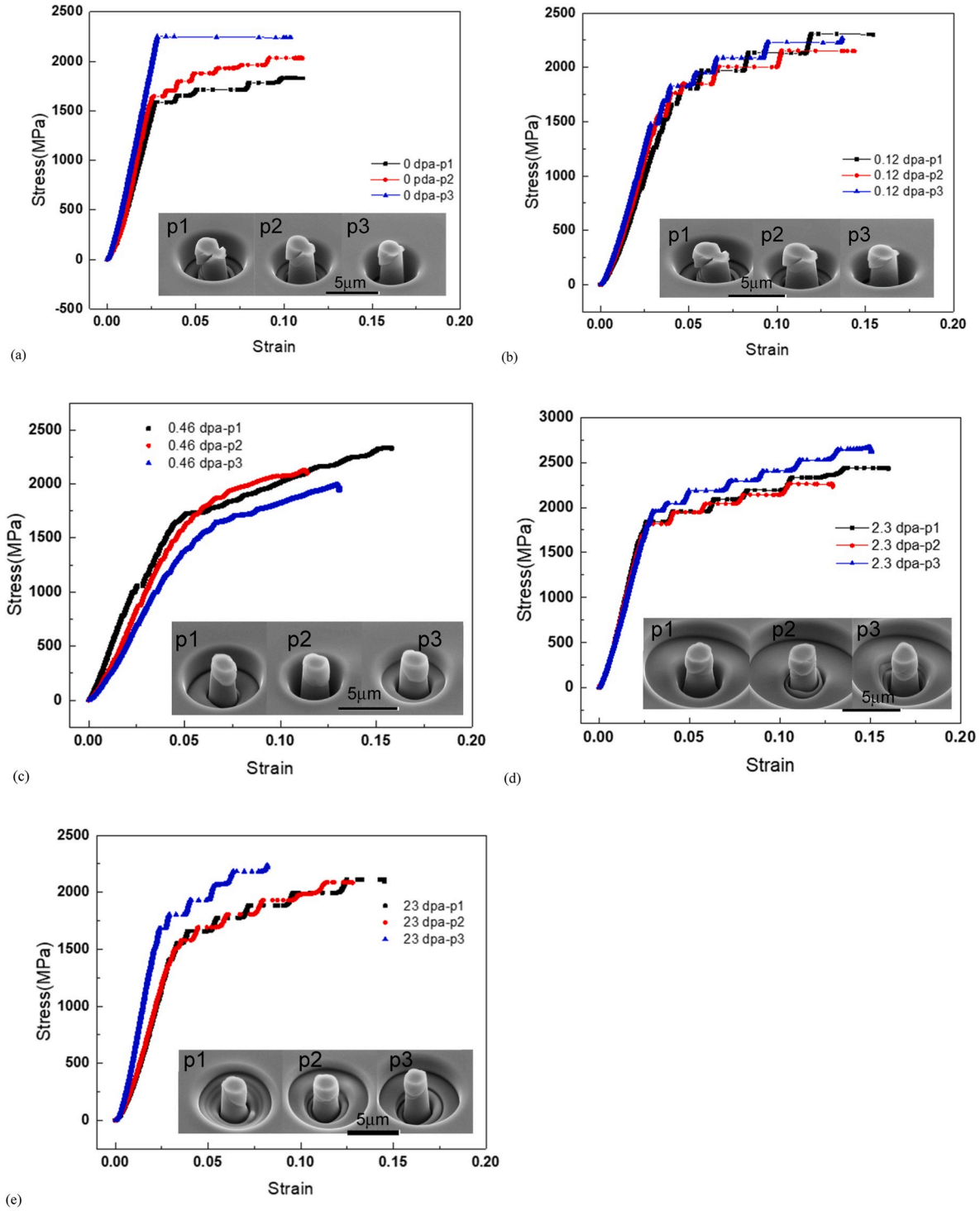

Fig. 9. Compressive engineering stress-stain curves of (a) the unirradiated sample and the samples irradiated to (b) 0.12 dpa, (c) 0.46 dpa, (d) 2.3 dpa and (e) 23 dpa. The SEM images of each deformed micropillar are inserted.

increases. As a result, the first pop-in becomes less detectable due to the machine limitation. A similar phenomenon of the pop-in vanish was also found in a Ti-based MG after ion irradiation [48]. Overall, it concludes that irradiation-induced rejuvenation results in a new state that has different types and characteristics of structural heterogeneities than the as-cast or annealed materials, but no crystallization is found in those samples after high dosage irradiation.

Again, this new state with different structural heterogeneities can also be verified from mechanical degradation, i.e., the decrease in elastic modulus and hardness. The elastic modulus of a material is determined by the atomic bonds that depend upon the interatomic distance. Therefore, the change in elastic modulus by irradiation is, in fact, the change in interatomic distance. Due to the irradiation induced defects with high free volume, the high-density defects eventually increase free volume in the material, thus increasing the atomic distance. In turn, the elastic modulus decreases with the increase of the irradiation-induced free volume. The change of interatomic distance could be further investigated by pair distribution function using synchrotron x-ray [49,

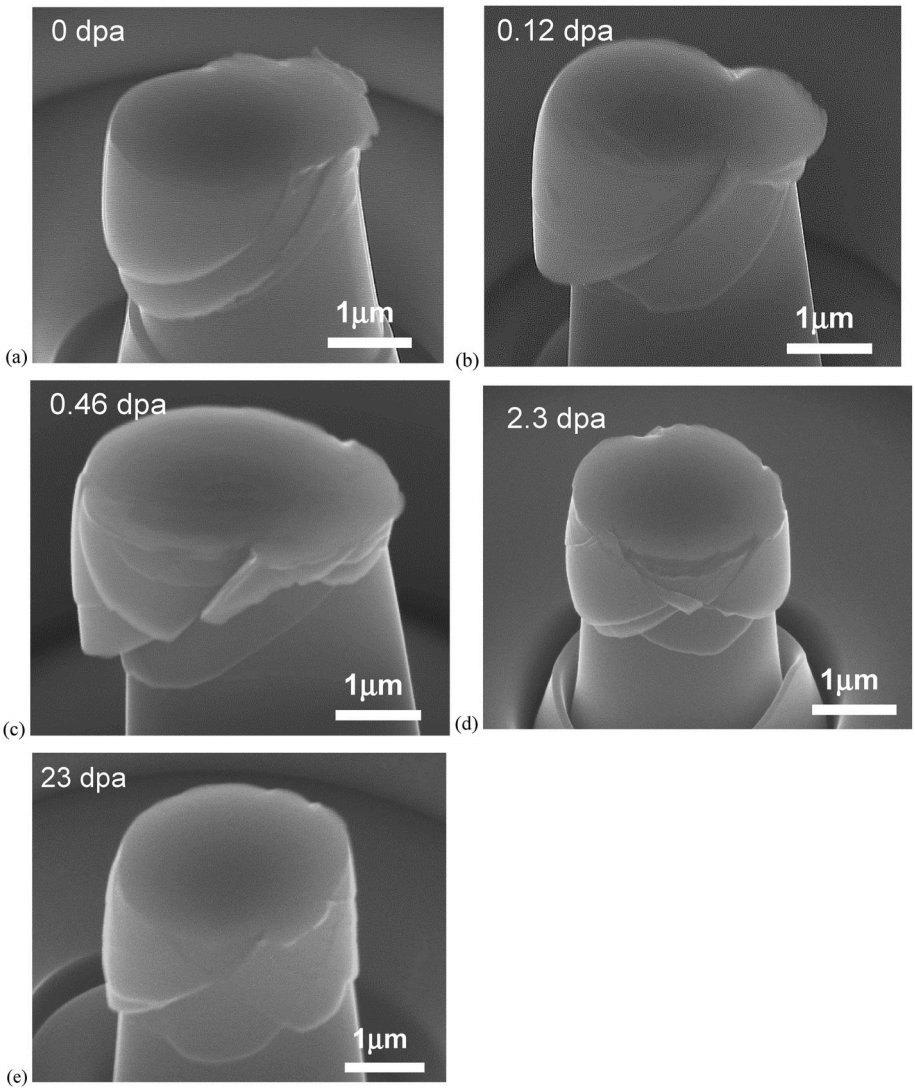

Fig. 10. Representative SEM images of the micropillar at irradiation doses of (a) 0 dpa, (b) 0.12 dpa, (c) 0.46 dpa, (d) 2.3 dpa and (e) 23 dpa in high resolution showing the shear band morphology after compression under a flat-ended indenter. One of three micropillars of each irradiation doses are illustrated here.

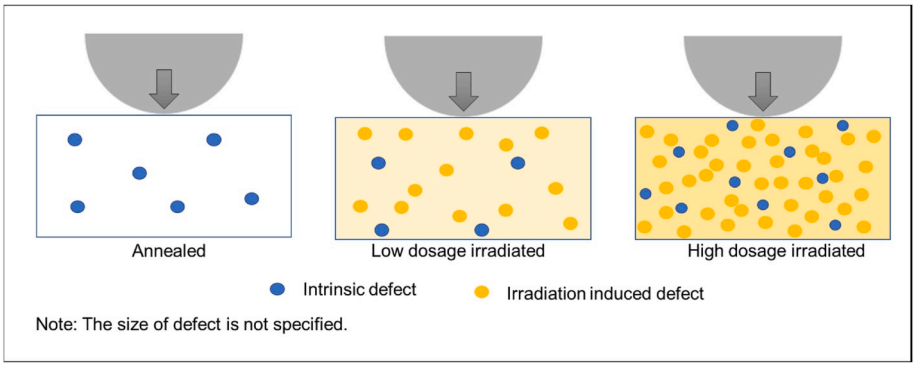

Fig. 11. Schematic illustration of irradiation induced defect and the structural changes indicating a transition from the annealed state, to an intermediate state, and finally to a different state of structural heterogeneities obtained in irradiated samples after relatively high-level irradiation.

50]. Meanwhile, the hardness reduction is attributed to irradiation defects. In micropillar compression tests, the shear band trends to initiate in soft spots, i.e., irradiation induced defects. Thus, high-density irradiation defects facilitate multiple shear band formation and their intersection in the sample irradiated to high dose as seen in SEM images of Fig. 10. Lacking microstructure as hindering propagation of shear bands, a dominant shear band leads to a shear crack rather readily, so that the shear band formed in the unirradiated sample and low-dose irradiated sample in Fig. 10 present a poor ductility. Increasing the possibility of intersections among shear bands is regarded as an effective

way to enhance ductility [51]. Thus, the observations of mechanical softening by nanoindentation and shear band intersection after micropillar compression indicate that irradiation not only increases defect density and free volume in the atomic scale but also increases plasticity in the macroscopic response. A similar structural transition was interpreted by the research of deformation mode in the MG nanowires using in-situ SEM mechanical testing [20], where the deformation was characterized as shear bands mediated in the as-molded sample and characterized as ductile at high ion fluences. Between the shear band mediated regime and ductile regime, an intermediate regime was observed as the fracture surface was not clearly a shear band or ductile mode, which indicates the transition of deformation modes.

The displacement excursion is an important indicator of a deformation mode of shear banding associated with elastic energy release. Generally, a shear band can only propagate an incremental distance if the strain energy relief associated with the propagation is larger than the energy increase of the shear band [52]. In the simplest analysis, the shear band propagates along the micropillar of an angle of 45°, relieving applied stress or strain. The elastic strain energy is decreased by an amount of $F\Delta x$ and the shear band energy is increased by an amount of $\sqrt{2}\pi d^2/4\Gamma$, where Γ is the energy per unit area of a shear band. A value Γ is estimated by the structural disordering [52]. Although larger plastic strain does not result in the further disordering of the structure, irradiation induced defects will increase the disordering, which is revealed from the increased FWHM at the dose higher than 2.3 dpa in Fig. 3. Since each displacement excursion corresponds to energy release by shear banding, analyzing the magnitude of excursion displacements is crucial in identifying the deformation mode. All the measurable displacement excursions are summarized as histograms in Fig. 12 and schematically fitted by Gaussian and exponential functions. As seen from Fig. 10, the excursion displacements were approximately described by a Gaussian function in the unirradiated sample with the peak displacement near 25–50 nm. After irradiation, the distribution of excursion displacements is changed. In the sample irradiated to 0.12 dpa, the histogram is illustrated by an exponential fitting where the most excursion displacements concentrate in small magnitude. As the irradiation is increased to 2.3 dpa, the histogram consists of a combination of Gauss-like distribution and exponential-like distribution, suggesting the structural transition induced by irradiation. When the sample is irradiated to 23 dpa, the excursion displacement distribution returns to a Gaussian distribution. However, the peak position and width are different from the unirradiated sample, indicating that this is a new state with different types and characteristics of structural heterogeneities induced by irradiation.

5. Conclusions

In this study, we investigated the ion irradiation effect on structural and mechanical changes in Zr-based MGs under different irradiation doses. Mechanical degradation and a transition to a new state with different structural heterogeneities were observed. The irradiation induced defects were quantitatively predicted by a statistic model unifying the thermal activated homogeneous nucleation of the shear band and defect-assisted heterogeneous nucleation of the shear band. The results and conclusions of the study are shown as follows:

(1) The XRD patterns indicate that fully amorphous structure after ion irradiation, while the structural discording was increased by irradiation as evidenced by the increase in FWHM.
(2) The reduction in modulus and hardness was observed after ion irradiation in nanoindentations tests and estimated by a simple model of the spherical indenter. The reduction was not significant until the irradiation dose exceeded 0.092 dpa.
(3) In the nanoindentation pop-in tests, the pop-in events vanished in the samples irradiated to high doses. The cumulative probability curves of τ_{max} for the first pop-ins indicated that the irradiated

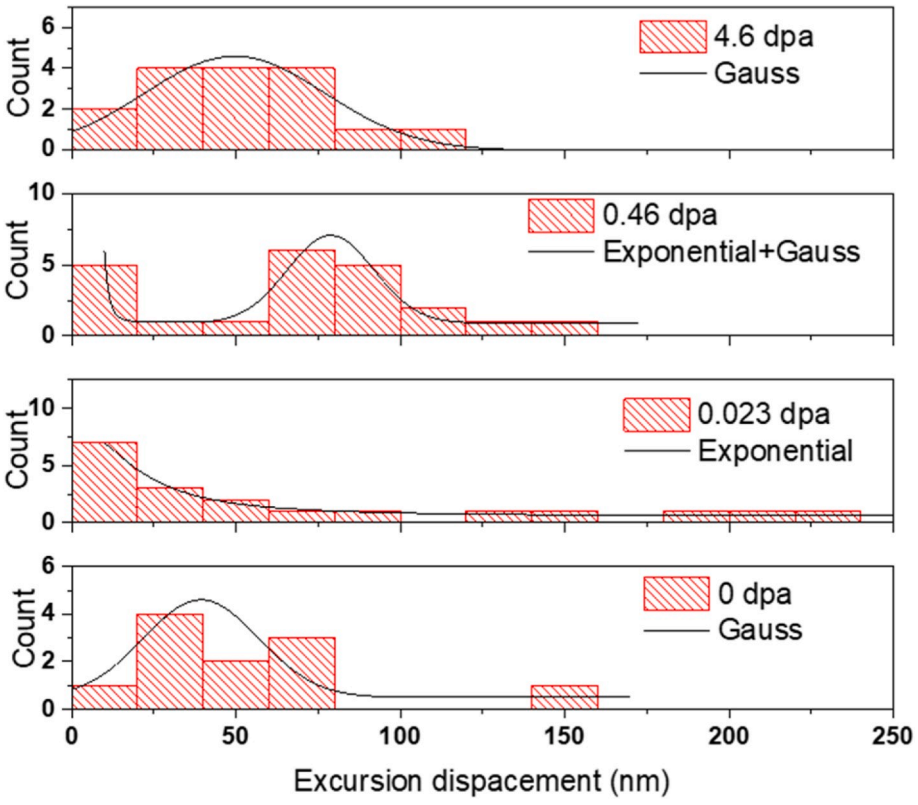

Fig. 12. Histograms of excursion displacement of micropillar compression tests in the sample irradiated to 0, 0.12, 2.3, and 23 dpa. The histogram is schematically fitted by Gaussian and exponential functions.

samples deformed more homogeneously than the unirradiated sample. By analyzing the cumulative probability curves by a unified statistic model, we proposed that the deformation of the unirradiated sample was governed by thermal activated homogeneous nucleation and pre-existing intrinsic detects simultaneously whereas the deformation of irradiated samples was completely dominated by the irradiation defects. Different from intrinsic defects in the annealed state, these irradiation-induced defects tended to reduce the strength as increasing irradiation doses.

(4) The shear band patterns after micropillar compression showed a transition of deformation modes from parallel non-intersecting shear bands to multiple intersecting shear bands as increasing the irradiation doses. The analysis of displacement excursion in micropillar compression confirms the transition of the structural state to a different state of structural heterogeneities.

Declaration of competing interest

The authors declare no competing interests.

CRediT authorship contribution statement

Tingkun Liu: Conceptualization, Investigation, Methodology, Writing - original draft, Writing - review & editing. **Wei Guo:** Conceptualization, Investigation, Methodology, Writing - original draft, Writing - review & editing. **Miguel L. Crespillo:** Conceptualization, Investigation, Methodology, Writing - original draft, Writing - review & editing. **Ke Jin:** Conceptualization, Investigation, Methodology, Writing - original draft, Writing - review & editing. **Yanwen Zhang:** Conceptualization, Investigation, Methodology, Writing - original draft, Writing - review & editing. **Hongbin Bei:** Conceptualization, Investigation, Methodology, Writing - original draft, Writing - review & editing. **Yanfei Gao:** Conceptualization, Investigation, Methodology, Writing - original draft, Writing - review & editing.

Acknowledgments

The authors are grateful to the support from the Center of Materials Processing at University of Tennessee (TL), the Governor's Chair Program at University of Tennessee (MLC and YZ), the internal funding from the School of Materials Science and Engineering at Zhejiang University (HB), and the US National Science Foundation DMR-1809640 (YG). Irradiations were performed using the instruments that were procured through the general infrastructure grant of DOE-Nuclear Energy University Program (DOE-DE-NE0000449).

Appendix A. Supplementary data

Supplementary data to this article can be found online at https://doi.org/10.1016/j.intermet.2020.106794.

References

[1] C.A. Schuh, T.C. Hufnagel, U. Ramamurty, Mechanical behavior of amorphous alloys, Acta Mater. 55 (2007) 4067–4109.
[2] A. Inoue, A. Takeuchi, Recent development and application products of bulk glassy alloys, Acta Mater. 59 (2011) 2243–2267.
[3] H.L. Jia, G.Y. Wang, S.Y. Chen, Y.F. Gao, W.D. Li, P.K. Liaw, Fatigue and fracture behavior of bulk metallic glasses and their composites, Prog. Mater. Sci. 98 (2018) 168–248.
[4] F. Spaepen, A microscopic mechanism for steady state inhomogeneous flow in metallic glasses, Acta Metall. 25 (1977) 407–415.
[5] A.S. Argon, Plastic deformation in metallic glasses, Acta Metall. 27 (1979) 47–58.
[6] M.L. Falk, J.S. Langer, Dynamics of viscoplastic deformation in amorphous solids, Phys. Rev. E 57 (1998) 7192–7205.
[7] E. Ma, Tuning order in disorder, Nat. Mater. 14 (2015) 547–552.
[8] N. Wang, J. Ding, F. Yan, M. Asta, R.O. Ritchie, L. Li, Spatial correlation of elastic heterogeneity tunes the deformation behavior of metallic glasses, npj Comput. Mater. 4 (2018) 19.
[9] X. Wang, W. Zhang, Y. Zhao, H. Bei, Y.F. Gao, Micromechanical investigation of the role of percolation on ductility enhancement in metallic glass composites, Mater. Sci. Eng. A 769 (2020) 138531.
[10] J. Saida, R. Yamada, M. Wakeda, S. Ogata, Thermal rejuvenation in metallic glasses, Sci. Technol. Adv. Mater. 18 (2017) 152–162.
[11] Y. Tong, W. Dmowski, H. Bei, Y. Yokoyama, T. Egami, Mechanical rejuvenation in bulk metallic glass induced by thermo-mechanical creep, Acta Mater. 148 (2018) 384–390.
[12] S. Ketov, Y. Sun, S. Nachum, Z. Lu, A. Checchi, A. Beraldin, H. Bai, W. Wang, D. Louzguine-Luzgin, M.A. Carpenter, Rejuvenation of metallic glasses by non-affine thermal strain, Nature 524 (2015) 200–203.
[13] M. Zhang, Y. Wang, F. Li, S. Jiang, M. Li, L. Liu, Mechanical relaxation-to-rejuvenation transition in a Zr-based bulk metallic glass, Sci. Rep. 7 (2017) 625.
[14] T. Nagase, T. Sanda, A. Nino, W. Qin, H. Yasuda, H. Mori, Y. Umakoshi, J. A. Szpunar, MeV electron irradiation induced crystallization in metallic glasses: atomic structure, crystallization mechanism and stability of an amorphous phase under the irradiation, J. Non-Cryst. Solids 358 (2012) 502–518.
[15] R. Gerling, F.-P. Schimansky, R. Wagner, Restoration of the ductility of thermally embrittled amorphous alloys under neutron-irradiation, Acta Metall. 35 (1987) 1001–1006.
[16] A.G. Perez-Bergquist, H. Bei, K.J. Leonard, Y. Zhang, S.J. Zinkle, Effects of ion irradiation on $Zr_{52.5}Cu_{17.9}Ni_{14.6}Al_{10}Ti_5$ (BAM-11) bulk metallic glass, Intermetallics 53 (2014) 62–66.
[17] Y. Zhang, T. Egami, W.J. Weber, Dissipation of radiation energy in concentrated alloys: unique defect properties and microstructural evolution, MRS Bull. 44 (2019) 798–811.
[18] Y. Zhang, R. Sachan, O.H. Pakarinen, M.F. Chisholm, P. Liu, H. Xue, W.J. Weber, Ionization-induced annealing of pre-existing defects in silicon carbide, Nat. Commun. 6 (2015) 8049.
[19] Y. Zhang, G.M. Stocks, K. Jin, C. Lu, H. Bei, B.C. Sales, L. Wang, L.K. Beland, R. E. Stoller, G.D. Samolyuk, M. Caro, A. Caro, W.J. Weber, Influence of chemical disorder on energy dissipation and defect evolution in concentrated solid-solution alloys, Nat. Commun. 6 (2015) 8736.
[20] D. Magagnosc, G. Kumar, J. Schroers, P. Felfer, J. Cairney, D. Gianola, Effect of ion irradiation on tensile ductility, strength and fictive temperature in metallic glass nanowires, Acta Mater. 74 (2014) 165–182.
[21] X.L. Bian, G. Wang, H.C. Chen, L. Yan, J.G. Wang, Q. Wang, P.F. Hu, J.L. Ren, K. C. Chan, N. Zheng, A. Teresiak, Y.L. Gao, Q.J. Zhai, J. Eckert, J. Beadsworth, K. A. Dahmen, P.K. Liaw, Manipulation of free volumes in a metallic glass through Xe-ion irradiation, Acta Mater. 106 (2016) 66–77.
[22] Y. Huang, H. Fan, X. Zhou, P. Xue, Z. Ning, D. Daisenberger, J. Sun, J. Shen, Structure and mechanical property modification of a Ti-based metallic glass by ion irradiation, Scripta Mater. 103 (2015) 41–44.
[23] E. Menéndez, A. Hynowska, J. Fornell, S. Suriñach, J. Montserrat, K. Temst, A. Vantomme, M. Baró, E. García-Lecina, E. Pellicer, Influence of the irradiation temperature on the surface structure and physical/chemical properties of Ar ion-irradiated bulk metallic glasses, J. Alloys Compd. 610 (2014) 118–125.
[24] Q. Xiao, L. Huang, Y. Shi, Suppression of shear banding in amorphous ZrCuAl nanopillars by irradiation, J. Appl. Phys. 113 (2013), 083514.
[25] S. Mayr, Impact of ion irradiation on the thermal, structural, and mechanical properties of metallic glasses, Phys. Rev. B 71 (2005) 144109.
[26] S. Michalik, J. Michalikova, M. Pavlovic, P. Sovak, H.P. Liermann, M. Miglierini, Structural modifications of swift-ion-bombarded metallic glasses studied by high-energy X-ray synchrotron radiation, Acta Mater. 80 (2014) 309–316.
[27] T.K. Liu, Y.F. Gao, H.B. Bei, Probing elastically or plastically induced structural heterogeneities in bulk metallic glasses by nanoindentation pop-in tests, AIP Adv. 7 (2017), 085216.
[28] W.D. Li, Y.F. Gao, H.B. Bei, On the correlation between microscopic structural heterogeneity and embrittlement behavior in metallic glasses, Sci. Rep. 5 (2015) 14786.
[29] J.R. Morris, H. Bei, G.M. Pharr, E.P. George, Size effects and stochastic behavior of nanoindentation pop-in, Phys. Rev. Lett. 106 (2011) 165502.
[30] Y.F. Gao, H. Bei, Strength statistics of single crystals and metallic glasses under small stressed volumes, Prog. Mater. Sci. 82 (2016), 18-150.
[31] C. Deng, C.A. Schuh, Atomistic mechanisms of cyclic hardening in metallic glass, Appl. Phys. Lett. 100 (2012) 25190.
[32] C.E. Packard, L.M. Witmer, C.A. Schuh, Hardening of a metallic glass during cyclic loading in the elastic range, Appl. Phys. Lett. 92 (2008) 171911.
[33] Y. Zhang, M.L. Crespillo, H. Xue, K. Jin, C.H. Chen, C.L. Fontana, J.T. Graham, W. J. Weber, New ion beam materials laboratory for materials modification and irradiation effects research, Nucl. Instrum. Methods B 338 (2014) 19–30.
[34] J.F. Ziegler, M.D. Ziegler, J.P. Biersack, SRIM – the stopping and range of ions in matter, Nucl. Instrum. Methods B 268 (2010) 1818–1823.
[35] W.J. Weber, Y. Zhang, Predicting damage production in monoatomic and multi-elemental targets using stopping and range of ions in matter code: challenges and recommendations, Curr. Opin. Solid State Mater. Sci. 23 (2019) 100757.
[36] H. Wiedersich, Effects of the primary recoil spectrum on microstructural evolution, J. Nucl. Mater. 179 (1991) 70–75.
[37] J.S. Field, M.V. Swain, A simple predictive model for spherical indentation, J. Mater. Res. 8 (1993) 297–306.
[38] S. Shim, H. Bei, M.K. Miller, G.M. Pharr, E.P. George, Effects of focused ion beam milling on the compressive behavior of directionally solidified micropillars and the

nanoindentation response of an electropolished surface, Acta Mater. 57 (2009) 503–510.
[39] W. Guo, E. Jagle, J.H. Yao, V. Maier, S. Korte-Kerzel, J.M. Schneider, D. Raabe, Intrinsic and extrinsic size effects in the deformation of amorphous CuZr/nanocrystalline Cu nanolaminates, Acta Mater. 80 (2014) 94–106.
[40] H. Bei, Z.P. Lu, S. Shim, G. Chen, E.P. George, Specimen size effects on Zr-based bulk metallic glasses investigated by uniaxial compression and spherical nanoindentation, Metall. Mater. Trans. A 41 (2010) 1735–1742.
[41] M.W. Thompson, Defects and Radiation Damage in Metals, Cambridge University Press, 1974.
[42] T. Egami, K. Maeda, V. Vitek, Structural defects in amorphous solids: a computer simulation study, Phil. Mag. A 41 (1980) 883–901.
[43] W. Luo, B. Yang, G. Chen, Effect of Ar+ ion irradiation on the microstructure and properties of Zr–Cu–Fe–Al bulk metallic glass, Scripta Mater. 64 (2011) 625–628.
[44] Y. Huang, B. Zhou, H. Fan, Y. Wang, D. Wang, J. Sun, J. Shen, Effect of ion irradiation in an $Al_{90}Fe_2Ce_8$ metallic glass, Mater. Des. 62 (2014) 133–136.
[45] S. Xie, E.P. George, Hardness and shear band evolution in bulk metallic glasses after plastic deformation and annealing, Acta Mater. 56 (2008) 5202–5213.
[46] H. Bei, S. Xie, E.P. George, Softening caused by profuse shear banding in a bulk metallic glass, Phys. Rev. Lett. 96 (2006) 105503.
[47] L. Wang, H. Bei, Y.F. Gao, Z.P. Lu, T.G. Nieh, Effect of residual stresses on the hardness of bulk metallic glasses, Acta Mater. 59 (2011) 2858–2864.
[48] A. Zare, Q. Su, J. Gigax, S. Shojaee, M. Nastasi, L. Shao, D. Lucca, Effects of ion irradiation on structural and mechanical properties of crystalline Fe/amorphous SiOC nanolaminates, Acta Mater. 140 (2017) 10–19.
[49] Y. Tong, T. Iwashita, W. Dmowski, H. Bei, Y. Yokoyama, T. Egami, Structural rejuvenation in bulk metallic glasses, Acta Mater. 86 (2015) 240–246.
[50] W. Dmowski, Y. Yokoyama, A. Chuang, Y. Ren, M. Umemoto, K. Tsuchiya, A. Inoue, T. Egami, Structural rejuvenation in a bulk metallic glass induced by severe plastic deformation, Acta Mater. 58 (2010) 429–438.
[51] R. Raghavan, K. Boopathy, R. Ghisleni, M.A. Pouchon, U. Ramamurty, J. Michler, Ion irradiation enhances the mechanical performance of metallic glasses, Scripta Mater. 62 (2010) 462–465.
[52] C.A. Volkert, A. Donohue, F. Spaepen, Effect of sample size on deformation in amorphous metals, J. Appl. Phys. 103 (2008), 083539.